Tethered particle motion analysis of DNA-binding properties of architectural proteins

Valk, R.A. van der; Zarguit, I.; Laurens, N.; Dame, R.T.

Chapter 22

Tethered Particle Motion Analysis of DNA-Binding Properties of Architectural Proteins

Ramon A. van der Valk, Ilias Zarguit, Niels Laurens, and Remus T. Dame

Abstract

Architectural DNA-binding proteins are key to the organization and compaction of genomic DNA inside cells. Tethered particle motion (TPM) permits analysis of DNA conformation and detection of changes in conformation induced by such proteins at the single molecule level in vitro. As many individual protein–DNA complexes can be investigated in parallel, these experiments have high throughput. TPM is therefore well suited for characterization of the effects of protein–DNA stoichiometry and changes in physicochemical conditions (pH, osmolarity, and temperature). Here, we describe in detail how to perform tethered particle motion experiments on complexes between DNA and architectural proteins to determine their structural and biochemical characteristics.

Key words Tethered particle motion, DNA conformation, DNA bending, DNA stiffening, DNA wrapping

1 Introduction

1.1 Tethered Particle Motion

In tethered particle motion assays, a DNA molecule is tethered between a polystyrene bead and a glass surface, causing the bead to exhibit a restricted Brownian motion. The excursion of the bead reflects the properties of the DNA tether; it changes in response to altered effective DNA stiffness or DNA contour length following the binding of proteins. The motion of the bead over time can be followed by video microscopy, tracked, and quantitated in terms of root mean square (RMS) displacement, providing an indirect read-out of the DNA conformation. A decrease or increase in effective DNA stiffness or DNA contour length is observed as reduction or increase in RMS, respectively.

Tethered particle motion is a single-molecule technique, which provides information on the properties of individual tethered DNA molecules. Single-molecule techniques are a powerful addition to the conventional biochemistry toolkit as they permit analysis of

Remus T. Dame (ed.), *Bacterial Chromatin: Methods and Protocols*, Methods in Molecular Biology, vol. 2819,
https://doi.org/10.1007/978-1-0716-3930-6_22,

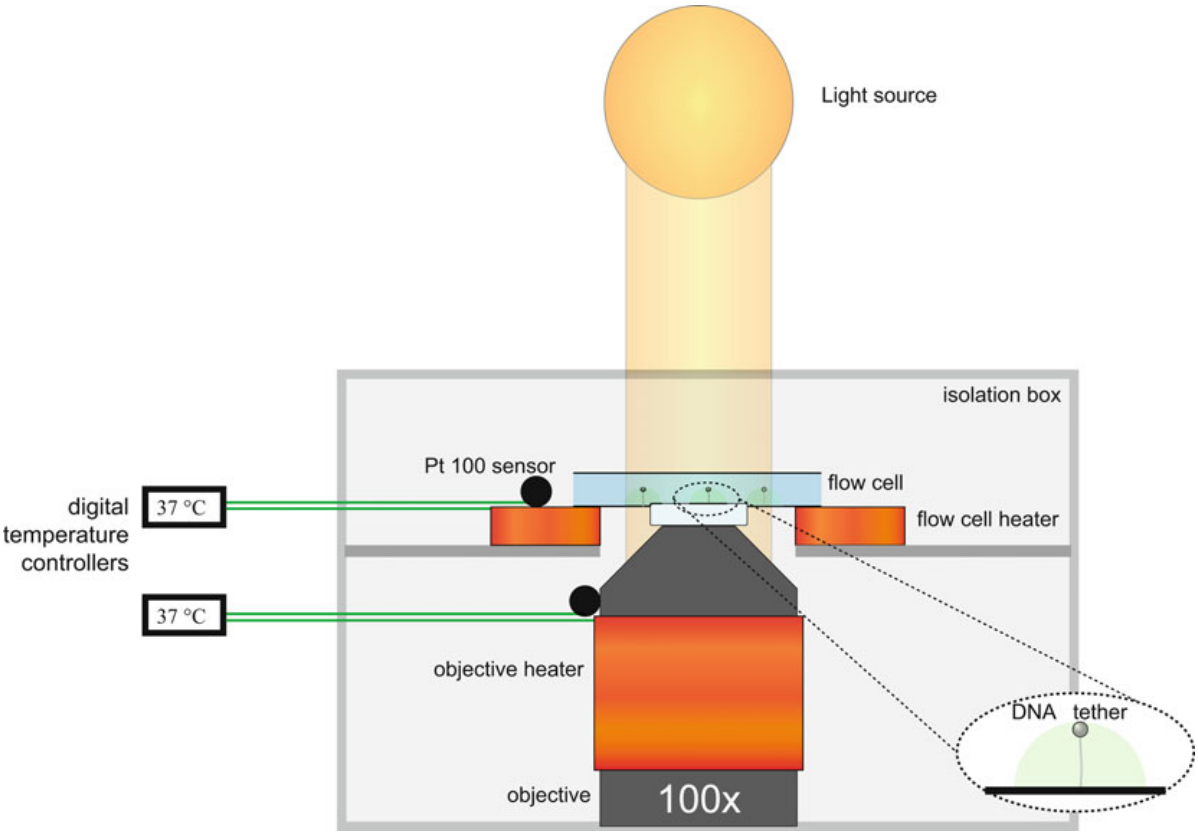

Fig. 1 Schematic overview of the tethered particle motion setup instrument with temperature control. The temperature of the incubation chamber is maintained by heating the flow cell holder (by surrounding the location of the flow cell with a heating element consisting of 40 parallel resistors (~5.5 watts)) and the objective (using an objective heating element (Bioscience tools TC-HLS-025)). The temperature is controlled by two SA200 PID digital temperature controllers, using pt100 sensors placed on the objective and on the edge of the flow cell heater. The system is insulated to ensure temperature stability [9]

populations of molecules without averaging, thus providing insight into the existence and characteristics of possible subpopulations. Different from more sophisticated single-molecule techniques (involving the application of force), TPM is easily implemented in any biochemistry lab; it only requires a microscope capable of imaging (sub)micron-sized beads and bead tracking software, resulting in low cost and low maintenance. Due to its simplicity it is also straightforward to integrate temperature control, a feature often overlooked in single-molecule instrumentation (Fig. 1). The absence of applied force, reducing the spatial resolution, makes data analysis more simple and straightforward compared to techniques involving application of force. However, the loss of this extra dimension within TPM is also its main limitation compared to single-molecule manipulation techniques, such as atomic force microscopy and optical and magnetic tweezers. TPM is therefore less suited for detailed quantitative analysis of DNA-binding enzymes which either apply or depend on force [1–4]. However, TPM is a powerful tool to analyze systems involving transient

looping of DNA tethers on the timescale of tenth of seconds to minutes and systems involving changes in the global properties of the DNA tether at equilibrium.

1.2 Tethered Particle Motion Studies of Architectural Proteins

TPM has proven to be very useful in quantitatively analyzing the behavior of proteins capable of DNA bridging, wrapping, and looping. In the latter case, using TPM, different looped states are observed as distinct RMS levels. Transition rates between these RMS levels yield quantitative insight in DNA looping kinetics [5–8]. The technique has also proven very useful in the characterization of the structural and biochemical properties of architectural proteins. TPM studies have shown that due to binding of proteins such as HU, Cren7, Sul7, Sso10a, NF-Y, HMfA/B, and TFAM, DNA attains a compact conformation, reflected in reduced RMS [9–13, 22]. The binding of proteins such as H-NS, HU, and Sso10a can (under certain conditions) result in an increased RMS, interpreted as protein–DNA filament formation [14, 15].

More in-depth quantitative analysis on the effect of the binding of different types of bacterial and archaeal architectural proteins on the RMS of a DNA tether can be found in Chapter 23.

2 Materials

Prepare all solutions using ultrapure water (prepared by purifying deionized water, to attain a sensitivity of 18 MΩ-cm at 25 °C) and analytical grade reagents. Prepare and store all stock solutions at −20 °C (unless indicated otherwise). You also need access to some routine biochemical techniques [16].

2.1 Stock Solutions

1. Sample Buffer (SB): 10 mM Tris–HCl pH 7.5, 150 mM NaCl, 1 mM EDTA, 1 mM DTT, 3% (w/v) glycerol, 100 μg/mL acytelated-BSA.
2. Passivation Solution (BGB): 4 mg/mL Blotting Grade Blocker Non-Fat Dry Milk (Biorad) or 2 mg/mL casein from bovine milk (Sigma-Aldrich) dissolved in SB (*see* **Note 1**).
3. Experimental Buffer (EB): This buffer corresponds with the chosen experimental conditions. Here we utilize buffers containing 10–25 mM Tris–HCl pH 7.0–7.5 and 75 mM KCl.

2.2 Generation of DNA Substrates Using PCR

To generate a DNA substrate for TPM we use polymerase chain reaction.

1. A DNA template containing the sequence of interest (in this example we generate a sequence of 685 bp in length using the pRD118 plasmid as a template; the plasmid is available upon request).

Table 1
Primer sequences

Primer name	Sequence	Modification
32% GC 685 bp Fw	ATACATATGCAACTTGAACGGCGTAAAAGAGGAACAATGG	5′ biotin
32% GC 685 bp Rev	GGTGGATCCTTTTCATCCCTTTAGTTCTTCCAG	5′ Dig

2. ‘5 biotinylated primer (Table 1).
3. ‘5 digoxygenin labeled primer (Table 1).
4. Phusion polymerase (Thermo Fisher).
5. Deoxyribose nucleotide triphosphate (dNTP).
6. Phusion 5× High-Fidelity Buffer (Thermo Fisher).
7. Gene elute PCR cleanup kit (Sigma-Aldrich) (*see* **Note 2**).
8. Eppendorf® PCR tubes.
9. Biorad C1000 Touch™ Thermocycler or any other available PCR machine.
10. 1% agarose gel in 1× TAE.
11. Nanodrop® or Qubit DNA quantification kit.
12. GeneRuler (Thermo Fisher).

2.3 Preparation and Assembly of Incubation Chamber

1. Anti-Dig 200 μg polyclonal antibodies (Roche).
2. Circular cover glasses with a diameter of 30 mm and 35 mm (*see* **Note 3**). If a dedicated holder as used in our lab is not available, regularly sized rectangular microscope slides and square cover slips can be used.
3. A method for cutting parafilm as described below.
4. Wattman paper.
5. 0.4–0.6 μm Streptavidin-coated polystyrene beads (G. Kisker GbR.).
6. Heating block capable of reaching 100 °C.
7. Fine pointed tweezers.
8. 90–100% ethanol.
9. Acetone.
10. Sonication bath.
11. KIMTECH precision wipes.
12. ShieldSkin orange nitrile™ 260.

2.4 Microscopy Equipment

1. TMC Vibracontrol clean top isolation table.
2. Inverted microscope Nikon Diaphot 300.

3. 100× oil-immersion objective (with a numerical aperture of at least 1.25).
4. Heat chamber.
5. Thorlabs CMOS camera DCC1545M.
6. Climatized room.
7. Nail polish/thermal glue.
8. Immersion oil.
9. Lens paper.

2.5 Particle Tracking and Analysis

1. Computer.
2. Particle tracking software. In our lab we employ the real-time particle tracking engine which is part of the software suite described by Sitters et al. and freely available online [17]. Other bead tracking algorithms can also be implemented and used. An objective comparison of particle tracking methods available is given by Chenouard et al. [18].
3. Custom MatLab routine (available upon request from the authors) for post-processing and analysis of raw *xy* position data.

3 Methods

3.1 Generation of DNA Substrates Using PCR

1. Reagents are combined in an Eppendorf® PCR tube according to the scheme below.

Reagent	Quantity
DNA template	1 ng
Forward primer	2.5 μL of 10 μM solution
Reverse primer	2.5 μL of 10 μM solution
dNTPs	5 μL of 2 mM solution
5× HF buffer	10 μL
Phusion polymerase	0.5 μL of 2 U/μL (1 enzyme unit)
H_2O	Add to total volume of 50 μL

2. This reaction mix is kept on ice as much as possible, and the PCR is initiated using the following protocol in a Biorad C1000 Touch™ Thermocycler.

Cycles	Temperature (°C)	Duration	Phase
1	98	1 min	Initialization
25	98	30 s	Denaturation
	65	30 s	Annealing
	72	1 min	Elongation
1	72	10 min	Final Elongation
1	15	∞	Hold

3. The PCR product is purified using the gene elute PCR cleanup kit (Sigma-Aldrich).
4. 2 μL of the purified PCR is loaded on a 1% agarose gel in TAE buffer alongside a DNA molecular weight marker for verification that a product of the expected length is formed.
5. An example of a successful PCR and purification of the obtained PCR product is shown in Fig. 2.

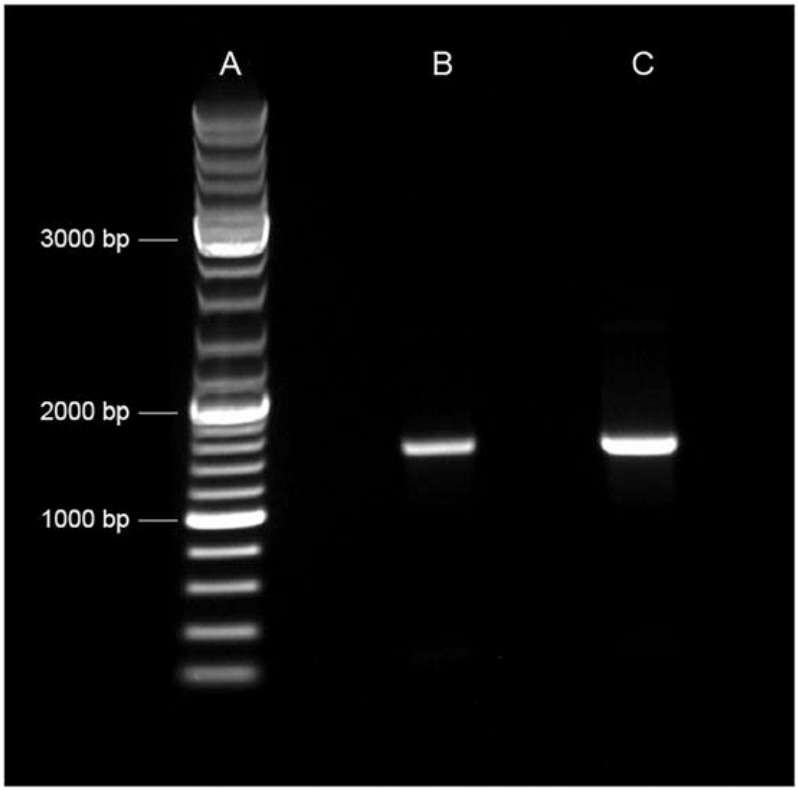

Fig. 2 1% agarose gel containing (**a**) 2 μL of the GeneRuler DNA molecular weight marker, (**b**) 2 μL of the PCR product, (**c**) and 2 μL of the purified DNA ready for use in tethered particle motion experiments. Even though the DNA substrate is 685 base pairs long, due to the addition of digoxigenin and biotin to the ends of the DNA construct, the substrate is shown to be heavier than 685 base pairs on gel

6. Finally, the concentration of purified PCR-generated DNA needs to be determined accurately. Use the Nanodrop® (or any other device capable of measuring UV absorbance) to estimate the purity (260/280) and concentration of the DNA. If no other method is available, the concentration of DNA can also be approximated using a DNA dilution series run on an agarose gel compared to a reference marker. Dilute the DNA in SB at a concentration of ~100–500 pM and store in aliquots at −20 °C.

3.2 Making Flow Cells

1. Before assembly of the flow cell, the cover glasses must first be cleaned thoroughly by submerging them in a beaker with acetone and placing the beaker in a sonication bath for 10 min followed by the same sonication procedure in ethanol. After the last sonication step, while wearing unpowdered gloves, gently dry the cover glass using KIMTECH precision wipes. Leave exposed to air for 10 min to dry completely.
2. To make the flow cells as displayed in Fig. 3, parafilm must be cut to the correct dimensions. The shape and size of the parafilm must be identical to the 30-mm cover glass except for a single 10-mm-wide channel running through the center. If possible, we advise to either use laser-cutting technology or a desktop cutting machine (such as aCameo Silhouette) to obtain the exact dimensions. Alternatively, parafilm can be cut by hand using a printed template and a scalpel.
3. Carefully align the parafilm to the edges of the 30-mm cover glass.
4. Sandwich parafilm between lower (large) and upper (small) round cover glass.
5. Compound the two halves by heating to 100 °C for 45–60 s, in between two massive metal blocks (Fig. 4) placed on top of a

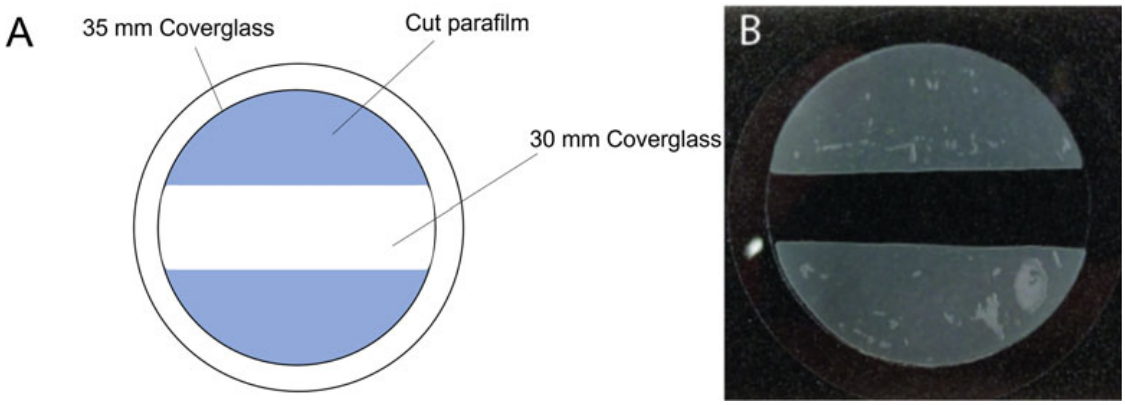

Fig. 3 TPM flow cell is made by sandwiching parafilm between two coverslip glasses and heating to melt the parafilm, causing it to act as a glue between the two glass coverslip glasses. (**a**) Schematic of a flow cell. (**b**) Picture of a flow cell

Fig. 4 Metallic plates made to hold and equally distribute heat and pressure when melting the parafilm and finalizing the flow cell

regular heating block. It is advised to apply a small amount of compression force to ensure that the halves are combined evenly. A complete flow cell can be seen in Fig. 3.

3.3 Preparing the Bead Solution

1. Dilute the beads to 0.01% w/v in SB.
2. Mix thoroughly using either a vortex or pipetting up and down.

   Sonicate with an immersion sonicator (Branson Digital Sonifier) with a fine point tip. Sonicate the diluted beads on ice at 25% with 2.5 ss on and 9.9 ss off for a total sonication time of 3 min (*see* **Note 4**).
3. Check the bead suspension by flowing 50 μL into a prepared flow cell and observing under the microscope while looking for bead clusters. If very few bead clusters, <1%, are observed, the bead stock is considered good for use; store at 4 °C.

3.4 Preparing Flow Cells

1. Wash and incubate the flow cell with 100 μL of **SB** containing 20 μg/mL of anti-dig for 10 min at room temperature.
2. Wash the flow cell with 100 μL of **BGB** buffer and incubate for 10 min at room temperature.
3. Wash the flow cell with 100 μL of **SB**.
4. Wash the flow cell with 100 μL of DNA solution (100–500 pM) diluted in **SB**; incubate for 10 min at room temperature.
5. Wash the flow cell with 100 μL of **SB**.
6. Wash the flow cell with 100 μL of bead solution.
7. Wash the flow cell with 100 μL of **EB**.
8. Wash the flow cell with 100 μL of protein solution (at the desired concentration) and incubate at room temperature for 10 min.
9. Wash the flow cell with 100 μL of protein solution (at the desired concentration) and seal the flow cell using nail polish.

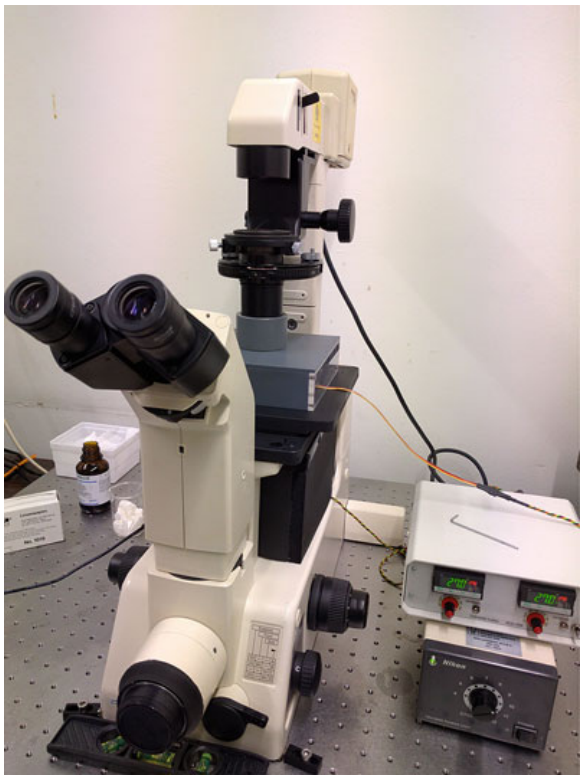

Fig. 5 Tethered particle motion instrument built on an inverted microscope. The flow cell is mounted on the microscope stage (not visible), which is embedded in an isolation chamber (center). The controller of the heating system (right) controls the temperature of the flow chamber as well as the objective used for imaging. Feedback ensures a temperature accuracy of 0.3 °C

3.5 Microscopy (for the Instrument See *Fig. 5)*

1. Place the flow cell in the holder (seen in Fig. 6).
2. Turn on the lamp and heating stage.
3. Place immersion oil on the objective (if needed), load the flow cell into the sample holder, and raise the objective until the beads come into focus.
4. Close the isolation chamber and wait for the temperature to stabilize. This may take 5–20 min depending on the desired temperature during the experiment; the system is at a stable temperature when no more focal drift is observed (*see* **Note 5**).
5. Verify sample quality by looking for moving beads (*see* **Note 6**).

3.6 Measurements

1. Select a region of interest in the field of view (as seen in Fig. 7), and track beads for a minimum of 1100 frames. Images are taken at 25 Hz, with a camera exposure time of 20 ms. Aim to measure at least 300 regions of interest per experimental condition to ensure sufficient "good" bead–tether combinations for quantitation after quality check (see below).

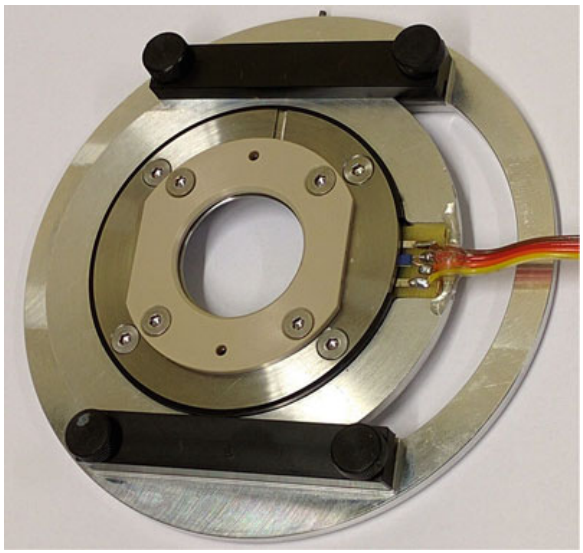

Fig. 6 Top view of the heated flow cell holder. The central part of the holder has some degrees of freedom to allow for the acquisition of multiple fields of view. The attachment point for the heat regulation is also visible

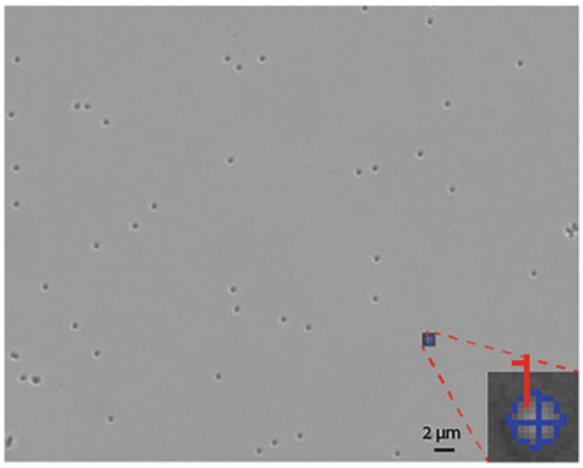

Fig. 7 Screen capture of a typical field of view with several surface tethered and moving beads. Individual beads are selected, and the position of the center of the beads is tracked over time

2. Determine the X and Y coordinates of the beads in the field of view using particle-tracking software. This can be done in two ways: (1) real-time particle tracking and (2) post-measurement particle tracking. Real-time analysis has the advantage of being able to directly verify the quality of the tracking. The downside of real-time particle tracking is that tracking many beads in parallel is computationally demanding. In our lab we employ the real-time particle tracking system, which is part of the software suite described by Sitters et al. and freely available online [17]. For other options, *see* Subheading 2.5.

3.7 Data Analysis

1. Calculate the anisotropic ratio—a measure of symmetry—of the scatterplots of the beads using Eq. 1. Exclude from further analysis beads with an anisotropic ratio greater than 1.2 as these are likely to be attached to multiple DNA tethers (*see* **Note 7**); a high anisotropic ratio may also result from poor surface passivation of the flow cell (*see* **Note 8**).

$$\alpha = l_{\text{major}}/l_{\text{minor}} \tag{1}$$

Equation 1: Calculation of anisotropic ratio (α), where l_{major} and l_{minor} represent the major and minor axis of the *xy*-scatterplot, respectively.

2. Calculate the RMS and the standard deviation of the RMS of the remaining beads.
3. Exclude all beads that have a standard deviation larger than 6% of their RMS (*see* **Note 9**). This is done to exclude beads that exhibit transient sticking to the surface of the flow cell. If you believe that transient shortening events may be occurring in your sample, please follow the instructions on "Highly dynamic DNA binding" described in Subheading 3.8.4.

$$\text{RMS} = \sqrt{\frac{1}{n}\sum_{i=1}^{n}\left[(x_i - \bar{x})^2 | + (y_i - \bar{y})^2\right]} \tag{2}$$

Equation 2: Calculation of the root mean squared displacement (RMS) using the x and y coordinates of the beads to discern the displacement.

To convert the measured RMS values of each bead to a single RMS value, the steps below need to be performed.

1. Make a histogram of all the RMS values for each experimental condition.
2. Fit the histogram using a Gaussian fitting curve to determine the average RMS and error (*see* **Notes 10** and **11**).

3.8 Analysis of Protein–DNA Complexes Using TPM

Architectural proteins can interact with DNA in a plethora of ways, resulting in different, distinct effects on RMS. The DNA-binding modes best studied by TPM are DNA bending, DNA wrapping, and multimerization along the DNA [19] (*see* **Note 12**). Some architectural proteins may exhibit sequence-specific interactions in addition to general nonspecific interactions. The structures formed upon binding at a specific high-affinity sequence may be distinct from the structures formed upon general binding to DNA. DNA binding may also occur in a cooperative or noncooperative manner. The degree of cooperativity can be determined using analysis methods described in Subheading 3.8.5. Furthermore, to give more insight on the protein–DNA interaction being studied, an end-to-end distance can be calculated and used for further analysis. Finally,

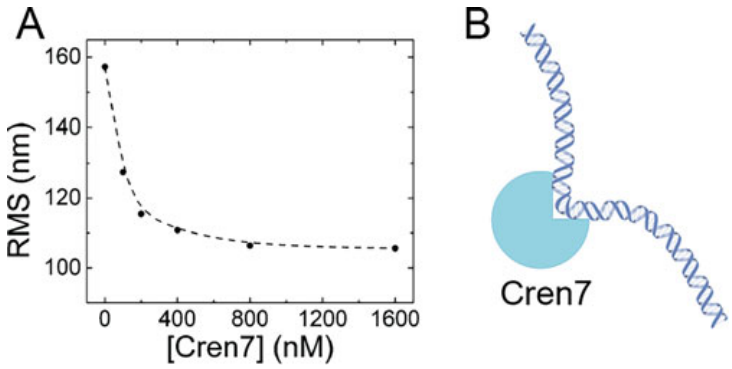

Fig. 8 Compaction of DNA by the DNA-bending protein Cren7. (**a**) Decrease of the root mean squared (RMS) displacement of the bead due to binding of increasing amounts Cren7. (**b**) Schematic model of DNA bending by Cren7

the protein–DNA complexes assembled upon protein binding may be highly dynamic, and depending on the relevant timescales, TPM is capable of sampling and quantifying dynamic changes. In Subheading 3.8.4 we will discuss strategies to not only measure but also quantify these effects. We will also discuss (in Subheading 3.8.5) how to relate RMS to more robust standards such as the persistence length of DNA.

3.8.1 DNA-Bending Proteins

DNA-bending proteins induce bends in DNA upon binding; these bends may be formed toward or away from the protein (*see* **Note 13**). Here we illustrate the effect of the binding of such proteins on the RMS using the noncooperative sequence unspecific DNA-bending protein Cren7 [20]. Titration of Cren7 yields a progressive concentration-dependent reduction in RMS of the tether from 160 nm to 110 nm, indicating DNA compaction due to DNA bending (Fig. 8).

3.8.2 DNA-Wrapping Proteins

A more extreme form of DNA bending is DNA wrapping. Here we illustrate the effects of DNA wrapping on the RMS using the archaeal histone protein HMfB from *Methanothermus fervidus*. HMfB protein dimers are able to stack upon each other, where DNA can wrap in a left-handed manner "infinitely" around the stacked HMfB histone core. The structure is further stabilized by hydrogen bonds and salt bridges between the stacked histone dimers. This quaternary structure of histone dimers and DNA is referred to as a hypernucleosome (Fig. 9a) [21, 22] . Titration of HMfA and HMfB results in a steep decrease in RMS, suggesting that HMf proteins exhibit high cooperativity in binding to DNA. Proteins yielding wrapped structures, such as hypernucleosomes, should compact DNA much more than DNA-bending proteins. Experimental data confirm this as the RMS value achieved at saturating conditions for HMf proteins is ~75 nm, which is significantly lower than the typical RMS found for DNA-bending proteins at

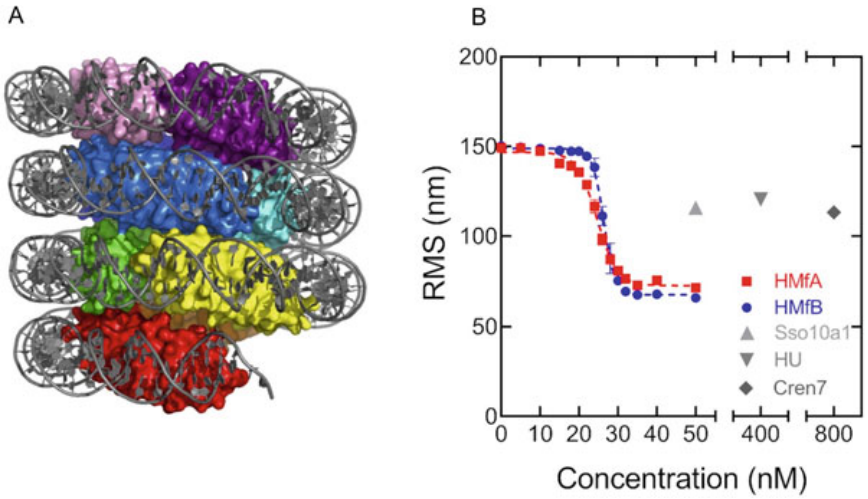

Fig. 9 Compaction of DNA by the DNA-wrapping protein HMfB. (**a**) Model depicting the hypernucleosome structure formed by HMfB. (**b**) Reduction of the root mean squared (RMS) displacement of the bead as a result of a titration with HMfA and HMfB in red and blue, respectively. Both proteins are able to compact DNA to extreme values, which can only be explained by hypernucleosome formation. In gray other DNA-bending proteins are shown at saturating conditions

saturating conditions (Fig. 9b) [figure taken from [21]]. Furthermore, by changing the DNA construct of interest or experimental buffer (EB) composition, it is possible to study the effect of DNA sequence specificity or environmental conditions on the protein of interest. For example, in Chapter 23 the authors demonstrate that there is a clear difference between the RMS response for HMfB on an aspecific DNA substrate and a SELEX-optimized DNA substrate.

3.8.3 DNA-Binding Proteins Capable of Multimerizing Along the DNA

Some proteins multimerize along DNA, using DNA as an assembly framework for multimer formation. An example of such a protein is H-NS. This protein exists as a dimer in solution, but depending on experimental conditions such as protein concentration or divalent/monovalent salts, it can either bridge DNA or form large multimers along DNA. Van der Valk et al. succeeded to demonstrate the DNA stiffening capabilities of H-NS by using TPM [14]. The multimerization of H-NS along a DNA molecule results in an increase in RMS from 145 nm to 165 nm (Fig. 10b). This significant increase in RMS demonstrates that H-NS is able to form a nucleoprotein along the DNA (Fig. 10b). Larger DNA substrates can also been used in TPM to demonstrate both DNA stiffening and bridging capabilities of H-NS (*see* **Note 12**).

3.8.4 Highly Dynamic DNA Binding

The structure of protein–DNA complexes can be highly dynamic. In that case it may be difficult to resolve the RMS of your bead using the standard analysis of your data. A clear indication of a

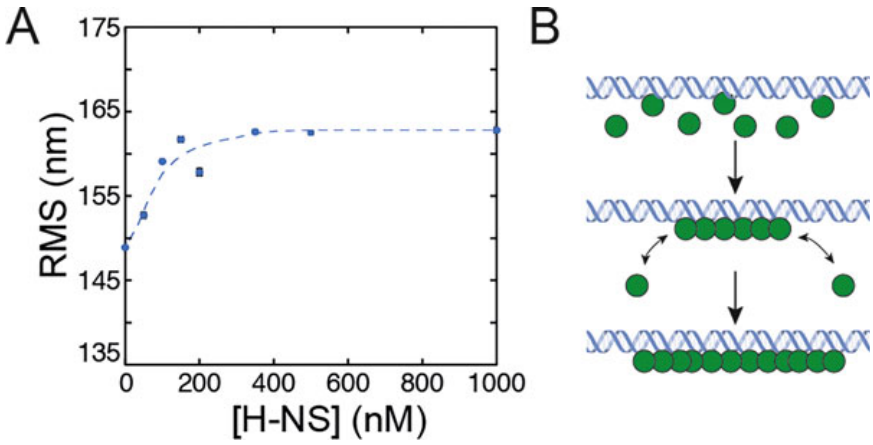

Fig. 10 DNA stiffening by H-NS. (**a**) Increase in root mean squared (RMS) displacement of the bead as a result of a titration with H-NS. (**b**) Model depicting the binding and multimerization along DNA

dynamic protein–DNA complex is that a large fraction of the tracked beads is discarded at the quality check stage. In such cases it is essential to confirm that particle disqualification is not a consequence of transient sticking of the bead to the glass surface (see above). Note that strong transient effects by the protein may be difficult to differentiate from random interactions of the bead with the surface. In such cases it is advised to confirm the observations using another technique.

For a good resolution of dynamic binding events or different DNA-binding modes, the measurement time frame may need to be extended. Exclude the time traces of beads with an anisotropic ratio exceeding 1.2. Calculate the RMS over time of these time traces using Eq. 3, which yields a moving average.

$$\mathrm{RMS}(t) = \sqrt{\frac{1}{150}\sum_{i=t}^{t+150}\left[(x_i - \bar{x})^2 | + (y_i - \bar{y})^2\right]} \qquad (3)$$

Equation 3: Dynamic calculation of RMS over time

Generate a histogram of the calculated RMS values. Different states in a measurement can be resolved if they represent a significant subpopulation of all states. Analysis of the data can be refined using a hidden Markov model [23] to determine the different RMS levels and their durations.

3.8.5 Further Analysis of DNA Binding

Although RMS is a quantitative unit of measure, it does not permit direct estimation of the protein (fractional) occupancy on the DNA. Based on fractional occupancy as a function of protein concentration, it would be possible to calculate k_d values. The fractional coverage can be calculated by the equation below, which is described in more detail by Driessen et al. [9]:

$$\text{Fractional coverage} = \frac{\sqrt{\frac{1}{L_p}} - \sqrt{\frac{1}{L_{p,bare}}}}{\sqrt{\frac{1}{L_{p,saturated}}} - \sqrt{\frac{1}{L_{-,bare}}}}$$

Here L_p represents the persistence length, $L_{p,bare}$ represents the persistence length of bare DNA, and $L_{p,saturated}$ represents the persistence length of the DNA–protein complex at saturated protein conditions. Based on simulations of the surface-tethered bead system, it is possible to convert RMS to *apparent* L_p, which can act as a proxy of the RMS (*see* **Note 14**). Following this conversion step, it is possible to quantitatively analyze the protein–DNA-binding curves to obtain DNA binding affinities (as described in Driessen et al. [9]). It is important to note that the RMS is dependent on the length of the DNA and the size of the beads used for TPM (*see* **Note 15**). It is therefore advised to perform these simulations (as described in [9]) matching the characteristics of the system investigated.

End-to-End Distance Calculation

More information than RMS alone can be retrieved from the tracked x and y positions. As the geometry of the experimental system is known, the end-to-end distance of the DNA or protein–DNA complex can be calculated. Specifically, such estimates provide useful information regarding the global structure of complexes between DNA and DNA-interacting proteins, in particular, DNA benders and wrappers.

By using the 5% most extreme deviations of each tracked bead independently, we are able to calculate the end-to-end distance with respect to the point where DNA anchors the measured bead (Fig. 11a [21]). At these extreme deviations the glass surface is limiting the bead to further move due to the diameter of the tethered bead (Fig. 11b [21]). As the x and y position as well as the mean radius of the bead is known, the end-to-end distance of the tethered DNA can be calculated by using Pythagoras' theorem and subtracting the average bead radius from the results.

For each bead, for every data point within the 5% most extreme deviations, the end-to-end distance is calculated and is plotted in a histogram. To achieve high precision, we recommend to perform this analysis on all the beads available. The histogram is subsequently fitted with a skewed Gaussian distribution (Fig. 11c [21]). The mean of the fit is determined to be the end-to-end distance, and the standard deviation of the fit represents the standard error. An example of the end-to-end distance calculation on data can be found in Chapter 23.

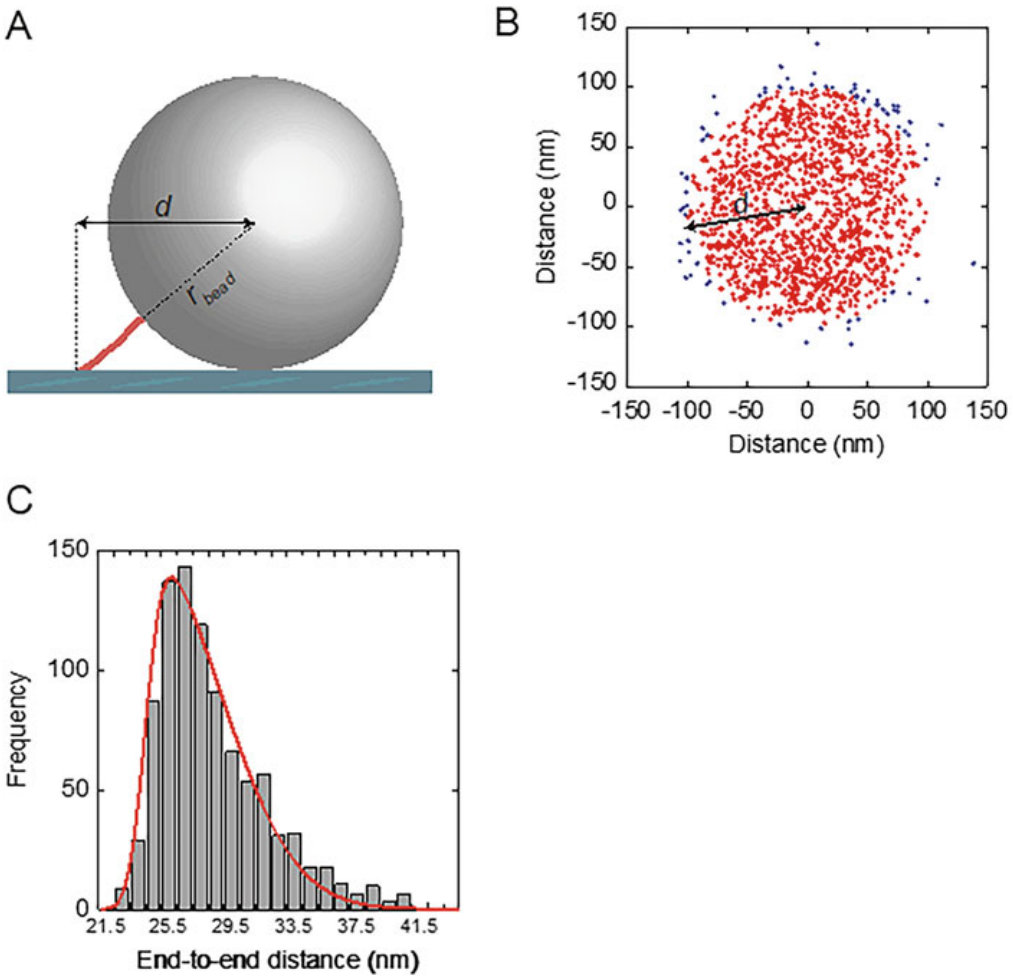

Fig. 11 End-to-end distance of relevant DNA-binding proteins. (**a**) The 5% most extreme values are used to calculate the end-to-end distance. (**b**) At the most extreme values the glass surface is limiting the polystyrene bead to further move due to the diameter of the tethered bead. Using Pythagoras' theorem we are able to calculate the end-to-end distance, represented in red. (**c**) For each datapoint the end-to-end distance is calculated and is plotted in a histogram, which is fitted by a skewed Gaussian distribution shown in red. The mean of the fit is the determined end-to-end distance, and the standard deviation represents the standard error

4 Notes

1. Before use, make sure to get rid of any insolubilized blotting-grade blocker or casein by spinning down insolubilized blotting-grade blocker/casein and passing the buffer through a filter.
2. Slightly different results in RMS values can be observed depending on which cleanup kit is used. The nature of these differences is unknown, but it is important to be consistent in the choice of cleanup kit used.
3. Although other shapes and types of cover glass can be used, in our hands these have shown the greatest ease of use.

4. Sonicating for longer than 5 min may damage the streptavidin-coated beads.
5. If after 20 min there is still drift observed, then most likely there is mechanical stress on the sample/flow cell. This means that there is something physically touching the sample and putting tension on it. Release this tension to get rid of the drift.
6. Tethered beads can be absent. In that case the quality and integrity of the DNA substrate can be verified by electrophoretic mobility shift analysis [16]. Incubate 2 μL of purified PCR product with either 2 μL of 20 μg/μL anti-digoxygenin or 2 μL of your bead stock. Load these samples on a 1% w/v agarose gel and visualize by staining (e.g., using ethidium bromide). The fraction of DNA shifted in the presence of either anti-digoxygenin or beads provides a quantitative measure of label presence and integrity.
7. Beads can be tethered to more than a single DNA molecule. This is visible as asymmetry in the *xy*-position plot of the bead. If a low fraction of the tethers exhibits this behavior, it is not a problem as these are discarded at quality control, by means of anisotropic cutoff. If it is a large fraction, the amount of DNA used in the assay needs to be reduced.
8. Beads can stick permanently or transiently to the glass surface. This indicates poor passivation of the glass surface and is undesired. Once a working protocol has been established, this may occur occasionally. If this occurs, the best solution is to discard the flow cell.
9. Both the anisotropic ratio and standard deviation values may need to be optimized depending on the system being investigated.
10. Beads can be tethered aspecifically. This is visible as a different RMS than expected for the length of the used tether. This would result in a wide distribution of RMS values in flow cells without DNA-binding proteins. If this occurs, it is advised to remake the DNA preparation from scratch.
11. When performing biological replicates, it is possible to calculate the average RMS values between the biological replicates. It is important however to perform a correct error propagation for the error.

$$\text{Error propagated standard deviation} = \sqrt{\frac{\sum_0^n \text{error}_n{}^2}{n}}$$

12. It is possible to measure both DNA stiffening and DNA bridging by H-NS using TPM. To make this possible, we have used a long DNA substrate of 3000 base pairs rather than the 685-base pair DNA substrate which is used by default.

However while both bridging and stiffening can be measured on this long DNA substrate, it is hard to quantitatively interpret the data on long tethers due to two modes of binding occurring concomitantly. As in any quantitative essay, it is essential to accurately determine protein concentration and to perform precise and reproducible serial protein dilution.

13. Poor reproducibility of data at a given protein concentration. This indicates surface binding of your protein. To counteract loss of protein of interest due to surface binding, BSA can be included in the experimental buffer.
14. Interpretation: caution is needed as observed effects on RMS may be due to different types of binding (e.g. DNA-bending or DNA-wrapping proteins), which cannot be directly discerned using TPM. As proteins binding to DNA will affect the persistence length of the DNA–protein complex being studied, L_p, each DNA binding type can have different effects on the L_p. It is therefore useful to first verify structural models using direct visualization techniques such as AFM [24, 25], (single molecule) FRET [26, 27], or conventional biochemical techniques before calculations for fractional occupancy are made.
15. The motion of a surface tethered bead is strongly dependent on the length of the DNA and the size of the bead. This implies that for each combination of DNA and beads, a separate simulation series is needed to establish the relationship between RMS and L_p.

Acknowledgments

Alson van der Meulen and Rosalie Driessen are acknowledged for optimizing experimental and analysis procedures used for TPM experiments. We would like to thank, in particular, Amanda Erkelens, Bram Henneman, Bert van Erp, Samuel Schwab, and Liang Qin, for streamlining and standardizing the TPM protocol within the lab.

This work was supported by the Netherlands Organization for Scientific Research [VICI 016.160.613/533 and OCENW.GROOT.2019.012 to RTD].

References

1. Neuman KC, Nagy A (2008) Single-molecule force spectroscopy: optical tweezers, magnetic tweezers and atomic force microscopy. Nat Methods 5(6):491–505. https://doi.org/10.1038/nmeth.1218
2. Herbert KM, Greenleaf WJ, Block SM (2008) Single-molecule studies of RNA polymerase: motoring along. Annu Rev Biochem 77:149–176. https://doi.org/10.1146/annurev.biochem.77.073106.100741
3. Bai L, Santangelo TJ, Wang MD (2006) Single-molecule analysis of RNA polymerase transcription. Annu Rev Biophys Biomol

Struct 35:343–360. https://doi.org/10.1146/annurev.biophys.35.010406.150153

4. Bustamante C, Macosko JC, Wuite GJ (2000) Grabbing the cat by the tail: manipulating molecules one by one. Nat Rev Mol Cell Biol 1(2):130–136. https://doi.org/10.1038/35040072
5. Beausang JF, Zurla C, Manzo C, Dunlap D, Finzi L, Nelson PC (2007) DNA looping kinetics analyzed using diffusive hidden Markov model. Biophys J 92(8):L64–L66. https://doi.org/10.1529/biophysj.107.104828
6. Laurens N, Bellamy SR, Harms AF, Kovacheva YS, Halford SE, Wuite GJ (2009) Dissecting protein-induced DNA looping dynamics in real time. Nucleic Acids Res 37(16):5454–5464. https://doi.org/10.1093/nar/gkp570
7. Laurens N, Rusling DA, Pernstich C, Brouwer I, Halford SE, Wuite GJ (2012) DNA looping by FokI: the impact of twisting and bending rigidity on protein-induced looping dynamics. Nucleic Acids Res 40(11):4988–4997. https://doi.org/10.1093/nar/gks184
8. Zurla C, Samuely T, Bertoni G, Valle F, Dietler G, Finzi L, Dunlap DD (2007) Integration host factor alters LacI-induced DNA looping. Biophys Chem 128(2-3):245–252. https://doi.org/10.1016/j.bpc.2007.04.012
9. Driessen RP, Sitters G, Laurens N, Moolenaar GF, Wuite GJ, Goosen N, Dame RT (2014) Effect of temperature on the intrinsic flexibility of DNA and its interaction with architectural proteins. Biochemistry 53(41):6430–6438. https://doi.org/10.1021/bi500344j
10. Driessen RPC, Lin SN, Waterreus W-J, van der Meulen ALH, Laurens N, Moolenaar GF, Wuite GJL, Goosen N, Dame RT (Accepted) Diverse architectural properties of Sso10a proteins: evidence for a role in chromatin compaction and organization. https://doi.org/10.1038/srep29422
11. Farge G, Laurens N, Broekmans OD, van den Wildenberg SM, Dekker LC, Gaspari M, Gustafsson CM, Peterman EJ, Falkenberg M, Wuite GJ (2012) Protein sliding and DNA denaturation are essential for DNA organization by human mitochondrial transcription factor A. Nat Commun 3:1013. https://doi.org/10.1038/ncomms2001
12. Guerra RF, Imperadori L, Mantovani R, Dunlap DD, Finzi L (2007) DNA compaction by the nuclear factor-Y. Biophys J 93(1):176–182. https://doi.org/10.1529/biophysj.106.099929
13. Nir G, Lindner M, Dietrich HR, Girshevitz O, Vorgias CE, Garini Y (2011) HU protein induces incoherent DNA persistence length. Biophys J 100(3):784–790. https://doi.org/10.1016/j.bpj.2010.12.3687
14. van der Valk RA, Vreede J, Qin L, Moolenaar GF, Hofmann A, Goosen N, Dame RT (2017) Mechanism of environmentally driven conformational changes that modulate H-NS DNA-bridging activity. elife 6. https://doi.org/10.7554/eLife.27369
15. Qin L, Ben Bdira F, Sterckx YGJ, Volkov AN, Vreede J, Giachin G, van Schaik P, Ubbink M, Dame RT (2020) Structural basis for osmotic regulation of the DNA binding properties of H-NS proteins. Nucleic Acids Res 48(4):2156–2172. https://doi.org/10.1093/nar/gkz1226
16. Sambrook J, Fritsch EF, Maniatis T (1998) Molecular cloning: a laboratory manual, 2nd edn
17. Sitters G, Kamsma D, Thalhammer G, Ritsch-Marte M, Peterman EJ, Wuite GJ (2015) Acoustic force spectroscopy. Nat Methods 12(1):47–50. https://doi.org/10.1038/nmeth.3183
18. Chenouard N, Smal I, de Chaumont F, Maska M, Sbalzarini IF, Gong Y, Cardinale J, Carthel C, Coraluppi S, Winter M, Cohen AR, Godinez WJ, Rohr K, Kalaidzidis Y, Liang L, Duncan J, Shen H, Xu Y, Magnusson KE, Jalden J, Blau HM, Paul-Gilloteaux P, Roudot P, Kervrann C, Waharte F, Tinevez JY, Shorte SL, Willemse J, Celler K, van Wezel GP, Dan HW, Tsai YS, Ortiz de Solorzano C, Olivo-Marin JC, Meijering E (2014) Objective comparison of particle tracking methods. Nat Methods 11(3):281–289. https://doi.org/10.1038/nmeth.2808
19. Dame RT (2008) Single-molecule micromanipulation studies of DNA and architectural proteins. Biochem Soc Trans 36(Pt 4):732–737. https://doi.org/10.1042/BST0360732
20. Driessen RP, Meng H, Suresh G, Shahapure R, Lanzani G, Priyakumar UD, White MF, Schiessel H, van Noort J, Dame RT (2013) Crenarchaeal chromatin proteins Cren7 and Sul7 compact DNA by inducing rigid bends. Nucleic Acids Res 41(1):196–205. https://doi.org/10.1093/nar/gks1053
21. Henneman B, Brouwer TB, Erkelens AM, Kuijntjes GJ, van Emmerik C, van der Valk RA, Timmer M, Kirolos NCS, van Ingen H, van Noort J, Dame RT (2021) Mechanical and structural properties of archaeal hypernucleosomes. Nucleic Acids Res 49(8):4338–4349. https://doi.org/10.1093/nar/gkaa1196

22. Henneman B, van Emmerik C, van Ingen H, Dame RT (2018) Structure and function of archaeal histones. PLoS Genet 14(9): e1007582. https://doi.org/10.1371/journal.pgen.1007582
23. Markov AA (1907) Investigation of a specific case of dependent observations. Izv Imper Akad Nauk (St-Petersburg) 3:61–80
24. Dame RT, Wyman C, Goosen N (2003) Insights into the regulation of transcription by scanning force microscopy. J Microsc 212 (Pt 3):244–253
25. Dame RT, van Mameren J, Luijsterburg MS, Mysiak ME, Janicijevic A, Pazdzior G, van der Vliet PC, Wyman C, Wuite GJ (2005) Analysis of scanning force microscopy images of protein-induced DNA bending using simulations. Nucleic Acids Res 33(7):e68. https://doi.org/10.1093/nar/gni073
26. Buning R, van Noort J (2010) Single-pair FRET experiments on nucleosome conformational dynamics. Biochimie 92(12): 1729–1740. https://doi.org/10.1016/j.biochi.2010.08.010
27. Dragan AI, Privalov PL (2008) Use of fluorescence resonance energy transfer (FRET) in studying protein-induced DNA bending. Methods Enzymol 450:185–199. https://doi.org/10.1016/S0076-6879(08)03409-5